New evidence for large earthquakes on the Central Iran plateau: palaeoseismology of the Anar fault

M. Foroutan, Michel Sébrier, H. Nazari, Bertrand Meyer, M. Fattahi, A. Rashidi, Kristell Le Dortz, D. Bateman

Geophysical Journal International

New evidence for large earthquakes on the Central Iran plateau: Paleoseismology of the Anar fault

Journal:	*Geophysical Journal International*
Manuscript ID:	GJI-S-11-0559.R1
Manuscript Type:	Research Paper
Date Submitted by the Author:	n/a
Complete List of Authors:	Foroutan, Mohammad; Université Pierre et Marie Curie, Paris 06, Institut des Sciences de la Terre de Paris UMR 7193 Sébrier, Michel; UPMC Paris6, Tectonique Nazari, Hamid; GSI Geological Survey oy Iran, Research Institute for Earth Sciences Meyer, Bertrand; Université Pierre et Marie Curie, Laboratoire de Tectonique UMR7072 Fattahi, Morteza; Oxford University, Centre for the Environment Rashidi, Ali; Geological Survey of Iran Le Dortz, Kristell; Universite Pierre et Marie Curie Bateman, Mark; Sheffield Centre for International Dryland Research, Geography
Keywords:	Palaeoseismology < SEISMOLOGY, Seismicity and tectonics < SEISMOLOGY, Asia < GEOGRAPHIC LOCATION

New evidence for large earthquakes on the Central Iran plateau: Paleoseismology of the Anar fault

Foroutan[1,2,3] M., M. Sébrier[2,3], H. Nazari[4], B. Meyer[2,3], M. Fattahi[5,6,7], A. Rashidi[8], K. Le Dortz[2,3,*] and M. D. Bateman[6]

1: Geological Survey of Iran, Azadi square, Meraj avenue, PO Box: 13185-1494, Tehran, Iran
email: foroutan@gsi.ir

2: UPMC Univ Paris 06, ISTEP UMR 7193, Université Pierre et Marie Curie, F-75005, Paris, France
email: mohammad.foroutan@upmc.fr, bertrand.meyer@upmc.fr, michel.sebrier@upmc.fr,

3: CNRS, ISTEP, UMR 7193, F-75005, Paris, France

4: Research Institute for Earth Sciences, Geological Survey of Iran, Po Box: 13185-1494,Tehran, Iran
email: h.nazari@gsi.ir

5: The Institute of Geophysics, University of Tehran, Tehran, Iran
email: mfattahi@ut.ac.ir

6: Sheffield Centre for International Dryland Research, Department of Geography, University of Sheffield, Winter Street, Sheffield S10 2TN, UK
email: M.D.Bateman@Sheffield.ac.uk

7: The School of Geography, University of Oxford, OX1 3QY, UK
email: morteza.fattahi@ouce.ox.ac.uk

8: Geological Survey of Iran, Postal Code 7615736841, Kerman, Iran
email: kermangeo@gsi-iran.org

* Now at: Laboratoire de Géologie, ENS, UMR 8538, 75231 Paris, ledortz@geologie.ens.fr

Abstract

The Central Iran plateau appears aseismic during the last few millenniums based on instrumental and historical seismic records. Nevertheless, it is sliced by several strike-slip faults that are hundreds kilometres-long. These faults display along-strike, horizontal offsets of intermittent gullies that suggest the occurrence of earthquakes in the Holocene. Establishing this is crucial for accurately assessing the regional seismic hazard. The first paleoseismic study performed on the 200-km-long, NS striking Anar fault shows that this right-lateral fault hosted three large ($M_w \approx 7$) earthquakes during the Holocene or possibly Uppermost Pleistocene for the older one. These three seismic events are recorded within a sedimentary succession, which is not older than 15 ka, suggesting an average recurrence of at

most 5 ka. The six OSL ages available provide additional constraints and allow estimating that the three earthquakes have occurred within the following time intervals: 4.4±0.8 ka, 6.8±1 ka, and 9.8±2 ka. The preferred age of the more recent event, ranging between 3600 yrs and 5200 yrs, suggests that the fault is approaching the end of its seismic cycle and the city of Anar could be under the threat of a destructive earthquake in the near future. Additionally, our results confirm a previous minimum slip rate estimate of 0.8±0.1 mm/yr for the Anar fault indicating the westernmost prominent right-lateral faults of the Central Iran plateau are characterized by slip rates close to 1 mm/yr. These faults, which have repeatedly produced destructive earthquakes with large magnitudes and long recurrence interval of several thousands of years during the Holocene, show that the Central Iran plateau does not behave totally as a rigid block and that its moderate internal deformation is nonetheless responsible for a significant seismic hazard.

Introduction

The Central Iran Plateau is a wide region experiencing low GPS deformation rates and is commonly described as a rigid block (e.g., Jackson & McKenzie, 1984; Vernant et al., 2004). The region (Figure 1) is nonetheless sliced by several strike-slip faults with clear morphological traces (Walker & Jackson, 2004; Meyer et al., 2006; Meyer & Le Dortz, 2007) that contrast with the very few earthquakes recorded in the region (Ambraseys & Jackson, 1998). Destructive earthquakes have occurred close to or along the Lut faulted borders only, and, according to the historical and instrumental records (Ambraseys & Melville, 1982; Ambraseys & Jackson, 1998), the prominent right-lateral strike-slip faults inland remained quiescent for millenniums. Although the absence of historical record of earthquakes in remote and uninhabited desert does not mean an absence of earthquakes, knowledge of the behaviour of such faults and assessment of the regional seismic hazard requires paleoseismic studies and depends on the selection of suitable trenching sites. This is the case for the region of the Dehshir and Anar faults. While a recent paleoseismic study stated the occurrence of large and infrequent earthquakes on the Dehshir fault (Nazari et al., 2009; Fattahi et al., 2010), the seismic behaviour of the Anar fault is still to be assessed.

The Anar fault is a 200-km-long NS strike-slip fault located nearby 55°E, in the middle of the Central Iran Plateau (Figure 1). The northern part of the fault is located within a mountainous region where several closely spaced splays cut across the Kuh-e Kharanaq range. The southern portion of the fault runs along the Kuh-e Bafq range and cuts right across the western piedmont of the range and across the Anar salt flat. The fault goes through the populated city of Anar and further bends eastwards to reactivate a thrust fault to the south. According to ^{10}Be cosmic ray exposure (CRE) and optically-stimulated luminescence (OSL) dating of cumulative offset of alluvial fans, the southern portion of the fault slips at a minimum rate of 0.8 mm/year (Le Dortz et al., 2009). Both the sharpness of these cumulative offsets and the absence of along fault microseismicity suggest these offsets have accrued through large and infrequent earthquakes rather than by creeping. At a few places, the offset of small gullies that ranges between 2.5 and 3.5 m (Figure 2) may be interpreted as the amount of coseismic slip during the last earthquake but clear evidence for a continuous and distinctive surface break is missing. Trenching appears therefore necessary to document earthquakes and access the Recent seismic history of the fault.

Site selection and trench stratigraphy

We scrutinized the fault on Quickbird satellite imagery and in the field to select the most favourable place to conduct paleoseismic investigations. The selected site is located 35 km north of the city of Anar along a very clear portion of the N175°E fault trace that is highlighted by an E-facing scarp (Figure 3). This fault scarp is readily seen cutting across numerous rills and ephemeral streams that incise a fan surface characterized by a subdued bar-and-swale morphology. The abandoned alluvial fan surface comprises a loose desert pavement of varnished clasts separated by sandy-silty material. The smooth scarp has a minimum height of 35 cm near the excavation (Figure 3b). South of the trench site, the scarp height increases progressively to reach one meter where small streams, which have been dammed and channelled along the fault, rejuvenate this scarp. North of the trench site, the scarp height also increases, but the streams are wider and deeper than to the south and have been able to maintain their courses to flow across the fault trace. At the trench site, the possibility of damming small intermittent streams during the emplacement of the fan material is high and the

possibility of subsequent erosion low, maximizing the chances to record the earthquakes coeval with alluvial aggradation and subsequent colluvial deposition. The next paragraphs report the observations gathered at the selected site, where trenching allowed us to distinguish three unambiguous events.

The eastern tip of the excavated trench is located about 5 km west of the Kuh-e Bafq range at 31.1953°N; 55.1536°E, and 1544-m-altitude above sea level (Figures 1 and 3b). The trench strikes N85°E, it has a 28-m-length, a depth between 4.3 and 4.7 m, and a width of some 1.5 m (Figures 3, 4, and 5). Trench walls expose a total deposit thickness of 5.9 m with fairly flat, 0.1-to 1-m-thick beds that correspond to medium-distal, alluvial fan facies. Trench stratigraphy is relatively straightforward as these beds are continuous and easily correlated across the fault zone located approximately in the middle of the trench (Figure 5). Overall the beds found in the trench are composed of sands and gravels mixed with variable amounts of silt and clay, these deposits correspond mostly to a debris-flow dominated alluvial fan. Although debris-flows and sheet-floods appears to dominate, sediment dynamics is not easy to determine precisely for each bed due to the medium-distal deposit conditions.

A total of 17 units have been defined in the excavated trench (see Table 1 and Figures 4 and 5). The uppermost part of the trench, approximately the last meter, is made of the thinner units 13 to 17 containing smaller pebbles than the alluvial units 1 to 8 and an almost clay-free matrix contrary to the units 9 to 11. This last meter hence is made of runoff deposits. The only evidence for a significant break in alluvial sedimentation is the ≈0.15-m-thick, gypsiferous calcrete that is located toward the top of unit 11. This latter unit and units 9 and 10 correspond to reddish brown, mud-dominated debris flows. OSL was used to date the alluvial layers seen in the trench.

OSL dating

Six lenses of fine sandy-silts intercalated between fanglomerates at various depths below the surface were sampled for OSL in opaque tubes (Figure 5). The Single Aliquot Regeneration (SAR) protocol (e.g.; Murray and Wintle, 2000) was employed for the Equivalent dose (De) measurement once quartz had been extracted and cleaned from each sample. The analytical procedures employed are identical to that applied to similar samples

from the neighbouring Sabzevar, Doruneh, and Dehshir faults (Fattahi et al, 2006; 2007; 2010; Le Dortz et al., 2011). In order to make all data consistent, three samples with ages that were previously published in Le Dortz et al. (2009), including one sample collected approximately 8 km farther north (OSL-2 on Figure 1 and in Table 2), have been refined in the light of procedural development outlined by Fattahi et al. (2010). Table 2 provides the relevant information for OSL ages in years from present (2010) with 1 sigma errors.

Initial attempts to use single grains for De determination failed due to the dimness of OSL signal. As a result, De measurements were undertaken on 9.6-mm-diameter aliquots containing approximately 1500-2000 grains. Whilst normally this might result in averaging out of any multiple dose component within a sample, here it is assumed that for these dim samples the luminescence signal from each aliquot was produced by a relatively few number of bright grains and thus may be considered as almost measuring at single grain level. Therefore, the De distribution of the single aliquot De measurements is considered to be almost a true reflection of the actual De distribution within a sample. For samples showing unimodal, apparently normally distributed De's with a low over-dispersion (Ant-I and Ant-IV in Table 2), which are interpreted as having had the OSL signal reset (bleached) prior to burial, Central Age Model (CAM) was employed for calculation purposes. For the remaining samples (Ant-II, Ant-III, Ant-V, Ant-VI and OSL-2 in Table 2), the depositional setting, field sedimentary logs, and the scatter of the replicate aliquot De data indicated that prior to burial, full resetting (bleaching) of the OSL signal had not taken place and/or that the sediments had undergone some post-depositional disturbance (Bateman et al., 2007). Indeed, the small size of the catchment area at the trench site, less than 20 km^2, is indicative of a rapid transport before the emplacement of the fan (Le Dortz et al., 2009). The great majority of the Anar trench deposits come from high-discharge depositional events with limited surface exposure, which favour partial bleaching (Rittenour, 2008). As a consequence, Finite Mixture Model (FMM; Roberts et al. 2000) was used where samples showed skewed, scattered, or multimodal distributions and the dominant De component was used for age calculations (as in Fattahi et al., 2010). This approach yielded ages in accordance with site stratigraphy except for sample Ant-III whose age was too young. This sample has exhibited the highest over-dispersion value (51%, Table 2) of all measured samples and three De component were extracted by FMM for this sample, the highest representing 30% of the signal and the smallest 47%. It is possible to get an age that fits with stratigraphy using the higher two De components extracted using FMM, corresponding to ages of 7.3±0.5 ka and 10.7±0.8 ka,

respectively. However, there are no good reasons to accept components representing only 23% or 30% of the data over the 47% of the data incorporated into the dominant smallest FMM component. The latter cannot be ignored on the basis of partial bleaching as it has a lower De and is unlikely to represent post-depositional disturbance as it is the dominant De component but also based on observed bedding within the unit. However, unlike most other samples studied, Ant-III was sampled actually on a stratigraphic boundary (between units 8 and 9). As the dose-rate for this sample is based only on the activity from unit 9, a difference in the gamma radiation dose received from unit 8 might help explain the apparent under-estimation of age based on the lowest FFM De component. Unfortunately field-based gamma-spectrometer readings or material for analyzing the radioactive elements within unit 8 were not available to test this and so the age of Ant-III has not been included within the subsequent site interpretation. Thus, the ages of the trench units have been constrained based on only five OSL ages (Ant-I, Ant-II, Ant-IV, Ant-V, and Ant-VI).

Ages of trench units

The samples collected within the trench define a time range spanning from 5.8 to 14.9 ka. The oldest age Ant-I (13.6±1.3 ka) stands at the bottom of the trench and belongs to one of the oldest stratigraphic units (unit 2), it indicates that all the trench units should be younger than 15 ka. As the youngest OSL sample Ant-VI (6.2 ± 0.4 ka) is located at 0.8 m below the surface (unit 14), these ages define a maximum time interval between 0 and 14.9 ka and a minimum one between 6.6 and 12.3 ka, indicating the trench deposits aggraded during the uppermost Marine Isotopic Stage 2 (MIS-2≈12-22 ka) and part, or the entirety of MIS-1. The age of the fan surface at the trench site appears poorly constrained between 0 and 6.6 ka.

A proxy to the surface age may be obtained by estimating average sedimentation rates. Assuming this fan surface is still active, the whole 5.9 m of sedimentary units seen in the trench should have been aggraded during the last 14.9 or 12.3 ka at an overall sedimentation rate ranging between 0.4 and 0.48 mm/yr. Deposit thicknesses above the samples Ant-I (13.6±1.3 ka) and Ant-II (12.4±0.6 ka) yield slightly lower rates ranging between 0.28 and 0.36 mm/yr. Conversely, if one assumes the top of the fan surface was abandoned just after 6.6 ka, the oldest possibility for the youngest sample (Ant-VI), the

sedimentation rate may have reached 1 mm/yr. These two extreme hypotheses raise the problem of the abandonment age of the alluvial fan at the precise location where the trench was excavated. The refined age of OSL-2 (10.1±0.6 ka versus 11.8 ±6.5 ka in Le Dortz et al., 2009), which is sampled some 8 km north of the trench (see location on Figure 1, see also Figures 4a and 7 in Le Dortz et al., 2009) at 0.8 m below the surface of another fan on the riser of a ≈4.5 m incised dry stream, suggests its surface was abandoned some 9-10 ka ago at this site while the fan surface at the trench site cannot be older than 6.6 ka. These ages are in agreement with the late Pleistocene and Holocene regional climate scenario, for the central and eastern Iran, as recently proposed by Walker & Fattahi (2011). In fact, the satellite image in the vicinity of the trench site (Figure 3a) shows this location corresponds to an area where the fan surface has been exceptionally preserved from the backward erosion of deeply incised dry streams. Therefore, the late aggradation on the fan surface at the trench site (~1544 m a.s.l.), resulting from surface runoff, lasted until more recently than some 8 km further north on a more proximal alluvial fan (~1748 m a.s.l.) where Le Dortz et al. (2009) collected the sample OSL-2. In conclusion, the best estimate for the aggradation rate of the trench sediments is provided by the depth difference of 3.3 m between Ant-I (13.6 ± 1.3 ka) and Ant-VI (6.2 ± 0.4 ka) samples, this rate ranges between 0.36 and 0.58 mm/yr. Interestingly, this rate is comparable to the late Pleistocene-Holocene aggradation rates derived from alluvial sediments in similar deposition settings at southwestern Nebraska, Negev desert and Central Iran plateau (Daniels et al., 2003; Guralnik et al., 2011; Schmidt et al., 2011). Consequently, the best averaged net sedimentation rate, if meaningful in such environment, amounts to 0.47±0.11 mm/yr suggesting that the final aggradation of the trench units ended between 3.6 and 5.2 ka to the west of the fault zone and approximately one thousand years later to the east of the fault zone. The abandonment age of the fan surface at the trench site (4.4±0.8 ka) is comparable with late Holocene drought cycles at 4.2 ka, proposed by Staubwasser et al. (2003) to the southeast of the Persian Gulf.

Seismic event identification

The surface geomorphology, particularly, the characteristics of the fault scarp, detailed geological and structural analyses of the trench walls (bed unconformities,

sealed fault strands, and fissure fills or sand-blows), and restoration of the trench log permit to trace three individual event horizons that correlate with three destructive past earthquakes, which ruptured the ground surface. The evidence for these three seismic events, which are labelled A, B, and C from the youngest to the oldest, is presented below.

Event A, the youngest event is responsible for the 35-cm-high, E-facing scarp, which is observed at the surface in the vicinity of the trench (Figures 3b and 3c). The trench log shows this scarp is located above a nearly 1-m-wide, steep faulted zone associated with an E-facing flexure of the upper trench units; i.e., downthrown to the east (Figure 5). Units 16 and 17 are not observed west of the fault zone nor warped eastward. They rest unconformably on unit 15 dipping about 25°E (Figure 6), hence indicating the faulting and flexuring deformation postdate unit 15 and predate units 16 and 17. As there are no significant thickness differences of the upper trench units on both sides of the fault zone, the faulting and flexuring deformation appear to result from a sudden and discrete slipping event on the fault zone instead of a continuous shear; i.e., creep slip (Figure 7-step 1). Inasmuch as the upper trench units are seen faulted up to unit 15, the discrete slipping event should relate to an earthquake that ruptured the surface producing the scarp. The event horizon of this earthquake locates on the top boundary of unit 15, so that it stands between this latter and units 16 and 17 to the east of the fault and corresponds approximately with the present-day topographic surface to the west of the fault. This suggests that the western block has been slightly eroded as well as partly concealed by units 16 and 17 so that its present-day height underestimates its original height at the time of the earthquake (Figure 7-step 2). Then, unit 17 is a local sag pond deposit caused by event A.

Backstripping of event A suggests its vertical throw is of some 60 cm (Figure 7-step 3), confirming that the 35-cm high scarp at the surface has been partly degraded. Taking into account the Anar fault is dominantly a strike-slip fault (Figure 2), the 60 cm of vertical displacement should be associated with at least a couple of meters of right-lateral displacement. Then, the magnitude of event A should be at least on the order of M_w 7. The age of event A is poorly constrained as the uppermost OSL sample (Ant-VI), which is at 0.8-m-depth, comes from unit 14. This indicates only that event A is younger than 6.6 ka. Tentatively, the sediment thickness, which stands between the sample Ant-

VI and the event horizon of event A, may be used to propose a rough estimate of the youngest possible age for this seismic event based on the aggradation rate between Ant-VI and Ant-I. Since aggradation of unit 15 ended between 3600 and 5200 years (see previous section) event A should not be younger than 3600 years and might be as old as 5200 years. This time interval will be considered as the preferred age of event A in the following discussion.

Event B, the penultimate event, is easily determined from analysis of the trench walls. Several filled fissures (unit 12), which postdate unit 11 and predate unit 13, are seen (Figures 5 and 7-step 4). A careful analysis of these filled fissures permits to conclude they correspond indeed to either open cracks or sand-blows (Figures 8a and 8b). It is possible to observe these features formed suddenly as they disrupt the hard gypsiferous calcrete (e.g., Figure 8b), which is located in the top part of unit 11. Thus, the interface between units 11 and 13 corresponds to the event horizon of event B. The backstripping analysis of the trench log (Figure 7), removing the effects of event A and the units aggraded between events A and B, allow reconstructing the event B horizon just after the penultimate earthquake (Figure 7-step 4). This reconstruction suggests that the rupture of event B should have occurred on two parallel fault strands of the Anar fault zone, totalling a vertical throw of some 40 cm, distributed into 25 cm on the eastern strand and 15 cm on the western one. Thus, the penultimate earthquake appears to have a vertical throw close to that of the last one, hence a magnitude lightly comparable with the one of event A. The age of event B is well constrained by three OSL ages (Ant-V, -IV, and -VI) and bracketed between 5.8 ka and 7.8 ka yielding an average age of 6.8±1 ka for this earthquake (Figure 9).

Event C, the oldest seismic event, can be safely identified on the trench walls. Evidence for a third earthquake rests on the facts that lower trench units (5 to 8) exhibit higher vertical throws than middle ones (9 to 11). Different reconstructions have been tested to restore the trench lower units, the best fit is obtained when considering the interface between units 8 and 9 as the event horizon of a surface rupturing earthquake (Figure 7-step 6). This reconstruction favours that event C ruptured along the eastern fault strand with a vertical displacement of about 25 cm. Nevertheless, this vertical displacement is poorly constrained and higher estimates might be obtained according to the amount of erosion chosen (dashed line on Figure 7-step 6). Even if this vertical

throw is poorly determined and appears smaller than the ones of the subsequent earthquakes, this does not imply a much smaller magnitude as the amount of coseismic vertical displacement is highly variable along a strike-slip fault (e.g., Barka, 1996; Barka et al., 2002). The age of event C is not well constrained, it occurred prior to the OSL age of sample Ant-V (7.1±0.7 ka) and after that of Ant-II (12.4±0.6 ka) so that it is bracketed within the interval between 6.4 and 13 ka, with a minimum interval of 4 ka (Figure 9). We have investigated the possibility for a fourth event in the lowermost part of the trench (Figure 5). However, the lowermost units (1 to 4) cannot be followed on the eastern side of the trench precluding the possibility to document an additional event.

Discussion and Conclusions

Due to the reduced size of the surface sag pond, a 3D trench exploration was not undertaken at the trench site so that the slip per event was not directly measurable for the three identified seismic events, A, B, and C. Accounting for the lack of morphological segmentation along the Anar fault (Le Dortz et al., 2009) and the excavation of a single trench, there are no possibilities to calculate confidently any magnitude. The restored vertical throws per event suggest only that the related magnitudes are more likely on the order of $M_w \approx 7$ (see previous section). The right-lateral offsets observed at the surface (Figures 2 and 3a) permit to reinforce this inference. Deeply incised intermittent streams are seen offset by 8±0.5 m (Le Dortz et al., 2009 and Figure 3a) while several weakly incised small dry gullies show offsets of 3±0.5 m only (Figure 2). Considering these lower offsets were more likely formed during the most recent earthquake, they provide the best estimate for the coseismic horizontal slip of event A. Such a coseismic slip at the surface agrees with a magnitude close to 7. Thus the higher offsets, which are only observed where the alluvial surface is older, should represent the cumulative horizontal slip of the last three events that are seen in the trench. Therefore, the three events, which are observed within the trench to the north of Anar city, should have had slip per event on the order of 3 m, suggesting they are of similar magnitudes.

Overall, the new data presented in this paper give evidence for at least three seismic events of similar sizes on the Anar fault (Figure 9). OSL age of Ant-I sample indicates that the aggradation of the trench units did not started much before 14.9 ka or

to the latest by 12.3 ka. Since only 3 events have occurred during the last 15 ka, this provides a rough estimate of at most 5 ka for the average maximum time interval between two earthquakes. The youngest age possibility may reduce this average time interval between two earthquakes to ≈4 ka. Considering the best estimates of average ages for the three seismic events A, B, and C are: 4.4±0.8 ka, 6.8±1 ka, and 9.7±3.3 ka, respectively (Figure 9), the time interval between two subsequent earthquakes is ill-defined and might vary significantly. Nevertheless, the average ages for events A, B, and C indicate that the intervals between two subsequent earthquakes should be of 2400 and 2900 years between events A-B and B-C, respectively. As the elapsed time since the last earthquake is 3600 years at least and 5200 years at most, this suggests we are getting close to the end of the seismic cycle and may anticipate a destructive earthquake for the Anar city in the near future.

Finally, the cumulative offset of 8±0.5 m (Le Dortz et al., 2009) postdating fan aggradation and the refined age of fan abandonment given by OSL-2 sample (10.1±0.6 ka) confirms a minimum slip rate estimate of 0.8±0.1 mm/yr for the Anar fault. Then, the westernmost prominent right-lateral faults of the Central Iran plateau, namely the Dehshir and Anar faults, which are active though void of historical and instrumental earthquakes, are characterized by slip rates close to 1 mm/yr (Le Dortz et al., 2009 and 2011). Such faults have repeatedly produced destructive earthquakes with large magnitudes (M_w≈7) and long recurrence interval of several thousands of years during the Holocene (Nazari et al., 2009; Fattahi et al., 2010 and this paper). This demonstrates that the Central Iran plateau does not behave totally as a rigid block and that its moderate internal deformation is nonetheless responsible for a significant seismic hazard.

Acknowledgements

This study benefited of the logistic and financial assistance from Geological Survey of Iran. Université Pierre et Marie Curie and INSU-CNRS provided complementary funding for the fieldwork and OSL measurements. M. Foroutan acknowledges a grant from the French Embassy in Tehran for part of his PhD thesis and complementary support from UPMC-ISTeP. David Lambert, Attaché Scientifique et

Culturel, is thanked for his continuing support to the cooperation between UPMC and GSI. M. Hosseini from Kerman GSI office helped with the logistics of the fieldwork. B. Oveisi, M. Nazem Zadeh, A. Agha Hosseini, and M.A. Shokri are thanked for various contributions to the fieldwork, H. Bani Assadi and M. Adhami for their safe driving in the field. M. Fattahi would like to thank the research department of the Tehran University. We thank two anonymous reviewers for helpful and constructive comments.

References

Ambraseys, N. & Melville, C., 1982. A history of Persian earthquakes. Cambridge University Press.

Ambraseys, N.N. & Jackson, J.A, 1998. Faulting associated with historical and recent earthquakes in the Eastern Mediterranean region. *Geophys. J. Int.* , 133, 390-406.

Barka, A.A., 1996. Slip distribution along the North Anatolian Fault associated with the large earthquakes of the period 1939 to 1967. *Bull. Seismol. Soc. Am.*, 86 (5), 1238–1254.

Barka, A.A., Akyüz, H.S., Altunel, E., Sunal, G., Çakir, Z., Dikbas, A., Yerli, B., Armijo, R., Meyer, B., De Chabalier, J.B., Rockwell, T., Dolan, J.R., Hartleb, R., Dawson, T., Christofferson, S., Tucker, A., Fumal, T., Langridge, R., Stenner, H., Lettis, W., Bachhuber, J. & W. Page, 2002. The Surface Rupture and Slip Distribution of the 17 August 1999 Izmit Earthquake (M 7.4), North Anatolian Fault. *Bull. Seismol. Soc. Am.*, 92, 43–60.

Bateman, M.D., Boulter, C.H., Carr, A.S., Frederick, C.D., Peter, D. & M. Wilder, 2007. Preserving the palaeoenvironmental record in Drylands: Bioturbation and its significance for luminescence derived chronologies. *Sedimentary Geology*, 195(1-2), 5-19.

Daniels, J.M., 2003. Floodplain aggradation and pedogenesis in a semiarid environment. *Geomorphology*, 56, 225-242.

Fattahi, M., Walker, R., Hollingsworth, J., Bahroudi, A., Nazari, H., Talebian, M., Armitage,

S., Stokes, S., 2006. Holocene slip-rate on the Sabzevar thrust fault, NE Iran, determined using Optically-stimulated Luminescence (OSL). *Earth and Planetary Science Letters,* 245, 673-684.

Fattahi, M., Walker, R.T., Khatib, M.M., Dolati, A. & A. Bahroudi, 2007. Slip-rate estimate and past earthquakes on the Doruneh fault, eastern Iran. *Geophy. J. Int.*, 168, 691-709.

Fattahi, M., Nazari, H., Bateman, M.D., Meyer, B., Sébrier, M., Talebian, M., Le Dortz, K., Foroutan, M., Ahmadi Givi, F. & M. Ghorashi, 2010. Refining the OSL age of the last earthquake on the Dheshir fault, Central Iran. *Quaternary Geochronology*, 5, 286-292, doi:10.1016/j.quageo.2009.04.005.

Guralnik, B., Matmon, A., Avni, Y., Porat, N., Fink, D., 2011. Constraining the evolution of river terraces with integrated OSL and cosmogenic nuclide data. *Quaternary Geochronology*, 6, 22-32.

Jackson, J. & D. McKenzie, 1984. Active tectonics of the Alpine-Himalayan Belt between western Turkey and Pakistan. *Geophys. J. R. Astron. Soc*., 77, 185-264.

Le Dortz, K., Meyer, B., Sébrier, M., Nazari, H., Braucher, R., Fattahi, M., Benedetti, L., Foroutan, M., Siame, L., Bourles, D., Talebian, M., Bateman, M.D. & Ghorashi, M., 2009. Holocene right-slip rate determined by cosmogenic and OSL dating on the Anar fault, Central Iran. *Geophys. J. Int.,* 179, 700-710.

Le Dortz, K., B. Meyer, M. Sébrier, R. Braucher, H. Nazari, L. Benedetti, M. Fattahi, D. Bourles, M. Foroutan, L. Siame, A. Rashidi, & M. Bateman, 2011. Dating inset terraces and offset fans along the Dehshir fault combining cosmogenic and OSL methods. *Geophys. J. Int.,* 185, 1147-1174.

Meyer, B., Mouthereau, F., Lacombe, O. & P. Agard, 2006. Evidence of Quaternary activity along the Deshir Fault, *Geophy. J. Int.*, 164, 192-201.

Meyer, B. & K. Le Dortz, 2007. Strike-slip kinematics in Central and Eastern Iran : estimating fault slip-rates averaged over the Holocene, *Tectonics*, 26, TC5009, doi:10.1029/2006TC002073.

Murray, A.S. & A.G. Wintle, 2000. Luminescence dating of quartz using an improved single-aliquot regenerative-dose protocol., *Radiation Measurements*, 32, 57-73.

Nazari, H., M. Fattahi, B. Meyer, M. Sébrier, M. Talebian, M. Foroutan, K. Le Dortz, M. D. Bateman & M. Ghorashi, 2009. First evidence for large earthquakes on the Deshir Fault, Central Iran Plateau. *Terra Nova*, 21, 417–426.

Rittenour, T.M., 2008. Luminescence dating of fluvial deposits: applications to geomorphic, palaeoseismic and archaeological research. *Boreas*, 37, 613-635.

R.G. Roberts, R.F. Galbraith, H. Yoshida, G.M. Laslett, J.M. Olley, 2000. Distinguishing dose populations in sediment mixtures: a test of single-grain optical dating procedures using mixtures of laboratory-dosed quartz. *Radiation Measurements,* 32 , 459-465.

Schmidt, A., Quigley, M., Fattahi, M., Azizi, Gh., Maghsoudi, M. and H. Fazeli, 2011. Holocene settlement shifts and palaeoenvironments on the Central Iranian Plateau: investigating linked systems. *The Holocene*, 21 (4), 583-595, DOI:10.1177/0959683610385961.

Staubwasser, M., Sirocko, F., Grootes, P.M. and M. Segl, 2003. Climate change at the 4.2 ka BP termination of the Indus valley civilization and Holocene south Asian monsoon variability. *Geophys. Res. Lett.*, 30(8), 1425, doi:10.1029/2002GL016822.

Vernant, P., Nilforoushan, F., Hatzfeld, D., Abbassi, M.R., Vigny, C., Masson, F., Nankali, H., Martinod, J., Ashtiani, A., Bayer, R., Tavakoli, F. & J. Chéry, 2004. Present-day crustal deformation and plate kinematics in the Middle East constrained by GPS measurements in Iran and northern Oman. *Geophy. J. Int.*, 157, 381-398.

Walker, R. & M. Fattahi, 2011. A framework of Holocene and Late Pleistocene environmental change in eastern Iran inferred from the dating of periods of alluvial fan abandonment, river terracing, and lake deposition, *Quaternary Science Reviews*, 30, 1256-1271, doi:10.1016/j.quascirev.2011.03.004.

Walker, R. & J. Jackson, 2004. Active tectonics and late Cenozoic strain distribution in central and eastern Iran, *Tectonics*, 23, TC5010, doi:10.1029/2003TC001529.

Figure captions

Figure 1. Landsat mosaic of the Anar fault area. White squares for location of photograph in Figure 2, Quickbird extract in Figure 3, and location of OSL-2 sampling site. Upper right inset locates the area within a simplified seismotectonic map of Iran. K, D, A, KB, N and G, respectively for Kashan, Dehshir, Anar, Kuh Banan, Nayband, and Gowk faults.

Figure 2. Field photograph of the Anar fault (vertical arrows, top panel) taken towards the north from 31.2764°N and 55.1304°E with emphasis on a 3 m right-lateral offset rill (horizontal arrow, bottom panel).

Figure 3. (a) Quickbird imagery of the Anar fault trace (red arrows) centred on the paleoseismological site (rectangle). Circle indicates the 8±0.5 m cumulative dextral-offset riser described as site 1 in Le Dortz et al. (2009). (b) Topographic DGPS map (top) and profiles (bottom) of the paleoseismological site. Contour interval is 5 cm (survey data not tied to absolute elevation). The smooth and subdued E-facing fault scarp is indicated by a red overprint and the location of the trench by a rectangle. Violet and green dots locate the DGPS data points used for the topographic profiles. (c) Field photograph, looking south, of the E-facing fault scarp. The upper part of the southern trench wall is in the foreground. Three white labels that are 1-m spaced show scale on trench wall.

Figure 4. Composite photomosaic of the sediments exposed in the Anar trench excavation, with top four meters (between 11 and 12 meters) east and bottom two meters (between 19 and 20 meters) west of the main fault zone (a), and corresponding stratigraphic log of the units with vertical positions of dated samples (b). Numbers indicate units described in detail in Table 1. Three event horizons (EH-A, -B and -C) are shown as thick black lines (see text for discussion). Stars locate the positions (see exact location in Figure 5) of the six samples with OSL ages given (c).

Figure 5. (Top) Photomosaic of southern trench wall (see Figure 3 for location). (Bottom) Corresponding log, with labels marking the stratigraphic units. Faults and fractures are shown with red and dashed red lines, respectively. Short black lines

represent bedding of sedimentary layers. Event horizons discussed in text are labelled as EH-A, EH-B and EH-C. Labelled black stars locate the OSL samples. Sample Ant-I, collected west of the fault zone at 4.1-m-deep within unit 2, yields an age of 13.6±1.3 ka. Sample Ant-II, collected east of the fault zone at 4.2-m-deep within unit 5, yields an age of 12.4±0.6 ka. Sample Ant-III, collected at 1.5-m-deep in a sandy lens of unit 9, yields a poorly constrain ages between 11.5 and 3.3 ka. Sample Ant-IV, collected at 1.5-m-deep at the base of a fissure filled with eolian and runoff sand deposits within unit 12, yields an age of 6.2±0.6 ka. Sample Ant-V, collected at 1-m-deep within unit 11, yields an age of 7.1±0.7 ka. Sample Ant-VI, collected at 0.8-m-deep in a sandy lens within unit 14, yields an age of 6.2±0.4 ka.

Figure 6. Photomosaic (top) and interpretation (bottom) of the main faulted zone showing evidence for the most recent earthquake (event A). Units 11 to 15, affected by faulting, are warped downward, while undeformed units 16 and 17 lie unconformably atop. Faults and tiny fractures are shown as red and dashed red lines, respectively.

Figure 7. Schematic view of possible restoration of trench log showing sequence of faulting and depositional phases from present-day (step 1) to prior to the oldest paleoearthquake (step 7). The trench log has been simplified for clarity. Dashed black lines show inferred ground surface prior to the erosion. Step 1) is present-day situation. Step 2) is E-facing fault scarp formed during the most recent earthquake. Step 3) is restoration of the ground surface to its position prior to event A showing a vertical displacement of about 60 cm created by faulting on the eastern branch. Step 4) is the penultimate earthquake denoted by open fissures and cracks formed near the main faulted zone. Sand-blows also emplaced in both sides and away of the main faulted zone. Step 5) is restoration of the ground surface to its position prior to event B showing vertical displacement created during penultimate earthquake on the eastern and western fault branches about 25 and 15 cm, respectively. Step 6) is the oldest earthquake, it has produced some surficial fissures within downthrown (eastern) block and a 25-cm-height E-facing fault scarp. Step 7) is restoration of the ground surface to its position prior to event C, showing a vertical displacement of about 25 cm.

Figure 8. Evidence for the penultimate earthquake (event B) encountered in a fissure fill and a liquefaction feature (sand-blow) at 16 and 22 meters of the trench log,

respectively. Red lines correspond to tiny cracks postdating the penultimate earthquake. (a) Photomosaic of fissure filled with eolian sands and silts and interpretative sketch. The fissure is ~85-cm-deep and up to ~55-cm-wide, tapering downward through unit 9. Colours denote stratigraphy as shown in Figures 4 and 5. The material at the base of the fissure includes a collapsed piece from sidewall and grades into interbedded sand and silt layers. The fissure is sealed by a grey, well-stratified, surficial runoff deposit (unit 13). (b) Photomosaic and interpretative sketch of a sand-blow (unit 12) made of sandy material of unit 8 injected into and deforming units 9 and 11. Hydraulic fractures, vertical and oblique alignments of dragged sands and gravels deform the host sediments close to the liquefaction pillar.

Figure 9. Five well-constrained OSL ages place bounds on the ages of the three paleoearthquakes (A, B, and C) identified in the Anar trench exposure. Light grey areas represent the maximum time windows for the past earthquakes, dark grey pointing the minimum time window for event C. For event A, hatched domain shows the preferred time interval of the earthquake (4.4±0.8 ka). Colour codes are similar to units shown in Figures 4 and 5. Question mark illustrates the ambiguity due to the lack of ages in units postdating the most recent earthquake (16 and 17).

Table 1. Detailed description of the units observed in the trench excavated across the Anar fault, corresponding stratigraphic column and log are shown in Figures 4 and 5, respectively.

Table 2. Calculated OSL ages on the Anar samples with their parameters. Ages have been calculated for quartz grains with size ranging between 90 and 150 microns.

Table 1

Unit	Detailed Stratigraphic Explanation
17	Light grey to cream, poorly stratified, silty sand with some angular gravels (20%, 0.5-2 cm).
16	Light cream, fairly stratified, medium consolidated, angular gravels (60%, 0.5-6 cm), with sand and silt matrix and some gypsiferous cementation.
15	Buff to light grey, well stratified, medium consolidated, angular gravels (50%, 0.5-10 cm), with sand and silt matrix and some gypsiferous cementation.
14	Grey to buff grey, thinly stratified, medium consolidated sand and angular granules (0.5-4 cm) with cross-bedding.
13	Grey, well stratified, medium to well consolidated, coarse sand with angular granules and few pebbles (30%, 0.2-6 cm). The unit bottom is erosive and rests both on units 12 and 11.
12	Light cream to grey, sandy fissure fills and sand-blows.
11	Brown to olive cream, roughly stratified, medium to well consolidated, silts and sands with some channels of angular gravels (40%, 0.1-4 cm). The top exhibits a hard gypsiferous calcrete.
10	Cream to grey, fairly stratified, poorly consolidated, coarse sands and angular gravels (50%, 0.1-3 cm) with sandy-silty matrix and some cross-bedding.
9	Reddish brown to brownish grey, non-stratified, semi-consolidated coarse sand, with clayish silt matrix, including some channels of angular gravels (90%, 2-15 cm) with silt matrix.
8	Cream to brownish grey, fairly stratified, well consolidated, angular granules and pebbles (60%, 0.2-3 cm), with silty sand matrix, including some small cobbles and traces of sulfate calcrete within the coarser levels.
7	Grey to brownish grey, poorly stratified, poorly sorted angular pebbles (70%, 0.5-10 cm), with sandy silt matrix.
6	Cream to brown, fairly stratified, angular granules and pebbles (80%, 0.2-4 cm), with silty sand matrix, including some sparse big cobbles and silty sand lenses.
5	Buff to light grey, fairly stratified, loose silt and sand.
4	Grey to light grey, poorly stratified, well sorted, silty sands with some cross-bedding and gravelly lenses.
3	Grey, fairly stratified, well consolidated, medium to well sorted, coarse angular gravels (90%, 0.5-10 cm) with silty sand matrix, including some sparse bigger cobbles and clayish silty sand lenses.
2	Grey, stratified, loose, silty sand, with some cross-bedding.
1	Grey, poorly stratified, well consolidated, angular pebbles (>20%, 0.5-3 cm) with silty sand matrix.

552 Table 2

553

Sample	Latitude ° N	Longitude ° E	Depth (m)	Water (%)	K (%)	U (%)	Th (%)	Annual dose rate (Gy/ka)	over-dispersion (%)	Skewness	CAM De (Gy)	FMM De (Gy)	Age (ka)
Ant-I (OSL1-b)*	31.1952	55.1534	4.1	2	0.93±0.03	1.16±0.05	4.0±0.1	1.64±0.05	24	0.69	22.3±1.90		13.6±1.3[a]
Ant-II	31.1952	55.1534	4.2	0.4	0.77±0.03	0.97±0.05	3.4±0.1	1.42±0.04	27	4.09	16.1±0.90	17.5±0.47	12.4±0.6[b]
Ant-III	31.1952	55.1534	1.7	1.1	0.97±0.01	1.23±0.05	4.3±0.1	1.75±0.04	51	2.1	9.7±1.09	6.1±0.24	3.5±0.2[b]
Ant-IV	31.1952	55.1534	1.5	0.6	0.94±0.01	1.44±0.05	3.7±0.1	1.78±0.14	20	0.01	11.0±0.61		6.2±0.6[a]
Ant-V	31.1952	55.1534	1.0	0.3	0.99±0.01	1.72±0.05	4.2±0.1	1.96±0.14	25	0.35	13.5±0.90	13.9±0.70	7.1±0.7[b]
Ant-VI (OSL1-a)*	31.1952	55.1534	0.8	0.6	1.21±0.01	1.60±0.05	5.9±0.1	2.20±0.05	42	0.94	11.6±1.39	13.7±0.56	6.2±0.4[c]
OSL-2	31.2697	55.1337	0.8	1.1	1.06±0.01	1.33±0.05	4.0±0.1	1.90±0.05	41	2.39	20.1±2.16	19.3±0.76	10.1±0.6[c]

554

555 [a] Age based on De determined using Central Age Model (CAM; Galbraith et al., 1999).

556 [b] Age based on De determined using the dominant component of Finite Mixture Modeling (FMM; Roberts et al., 2000).

557 [c] Age previously published, now refined using Finite Mixture Modeling (FMM; Roberts et al., 2000).

558 * Parenthesis contains the sample label used by Le Dortz et al. (2009)

559

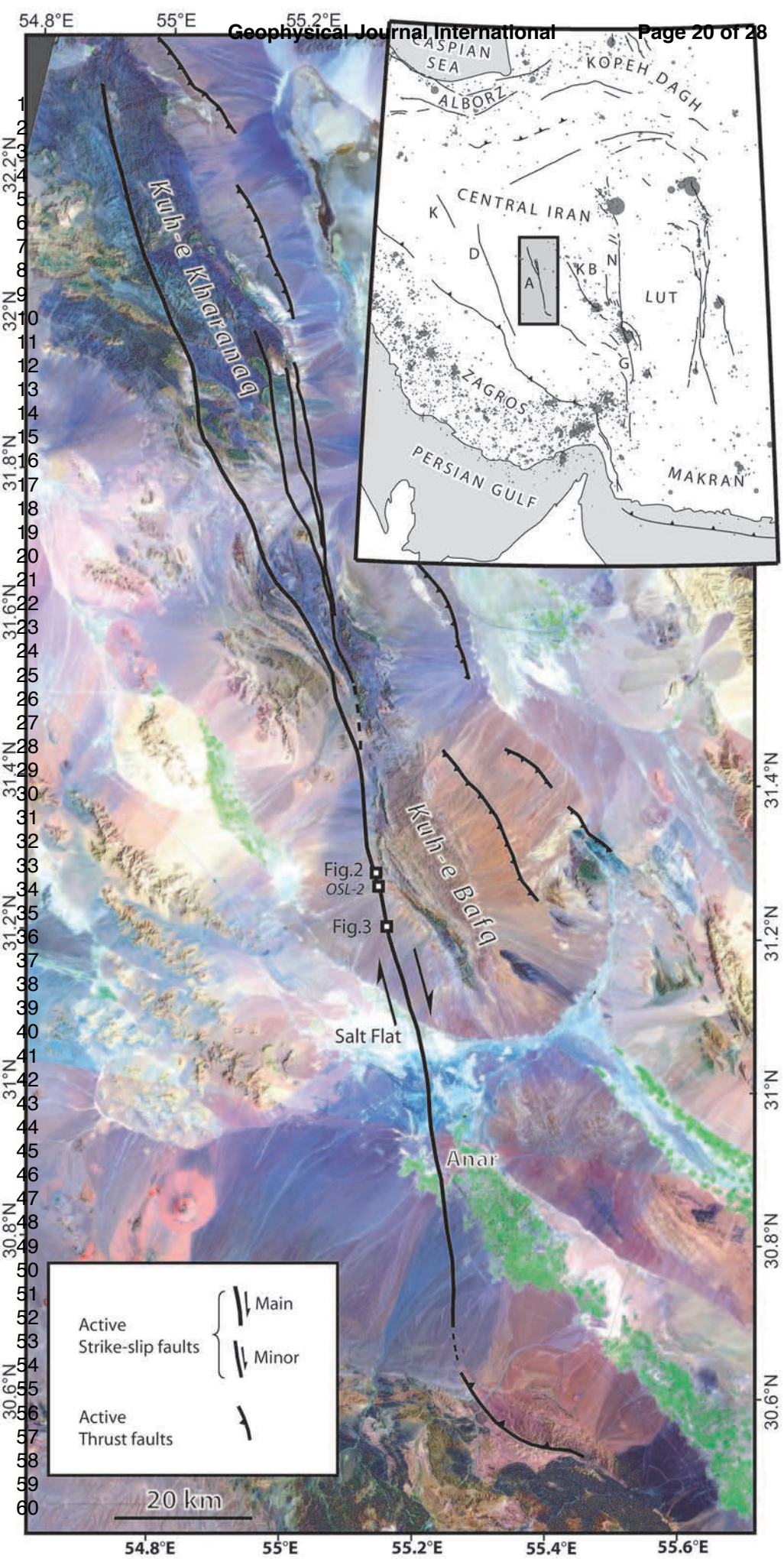
54.8°E
55°E
55.2°E
55.4°E
55.6°E
32.2°N
32°N
31.8°N
31.6°N
31.4°N
31.2°N
31°N
30.8°N
30.6°N
Kuh-e Kharanaq
Kuh-e Bafq
Fig.2
OSL-2
Fig.3
Salt Flat
Anar
CASPIAN SEA
ALBORZ
KOPEH DAGH
CENTRAL IRAN
K
D
A
KB
N
LUT
G
ZAGROS
PERSIAN GULF
MAKRAN
Active Strike-slip faults
Main
Minor
Active Thrust faults
20 km


W
E
S
N

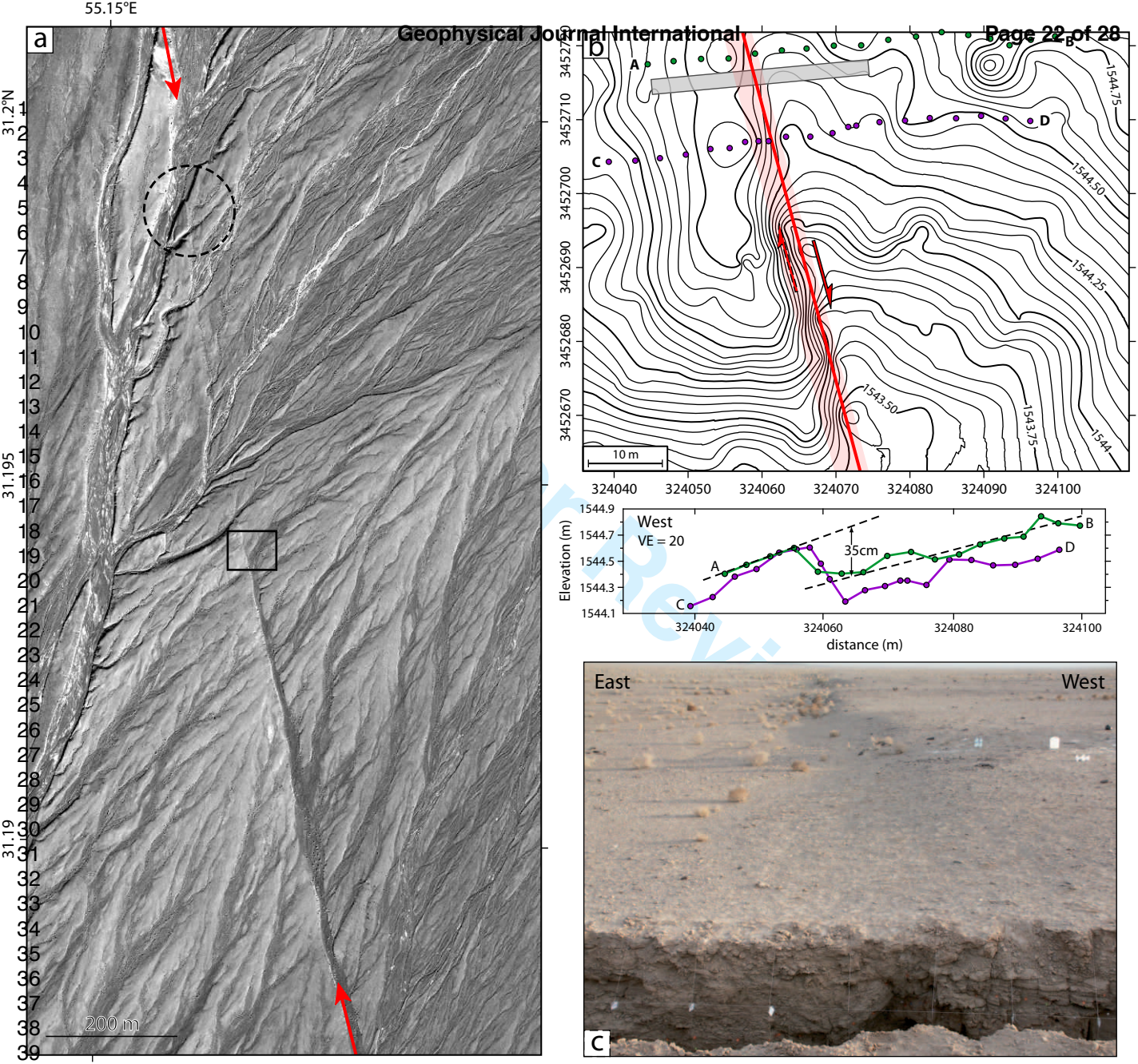
a
55.15°E
31.2°N
31.195
31.19
200 m
b
A
B
C
D
1544.75
1544.50
1544.25
1544
1543.75
1543.50
10 m
3452720
3452710
3452700
3452690
3452680
3452670
324040
324050
324060
324070
324080
324090
324100
West
VE = 20
35cm
Elevation (m)
1544.9
1544.7
1544.5
1544.3
1544.1
distance (m)
East
West
c

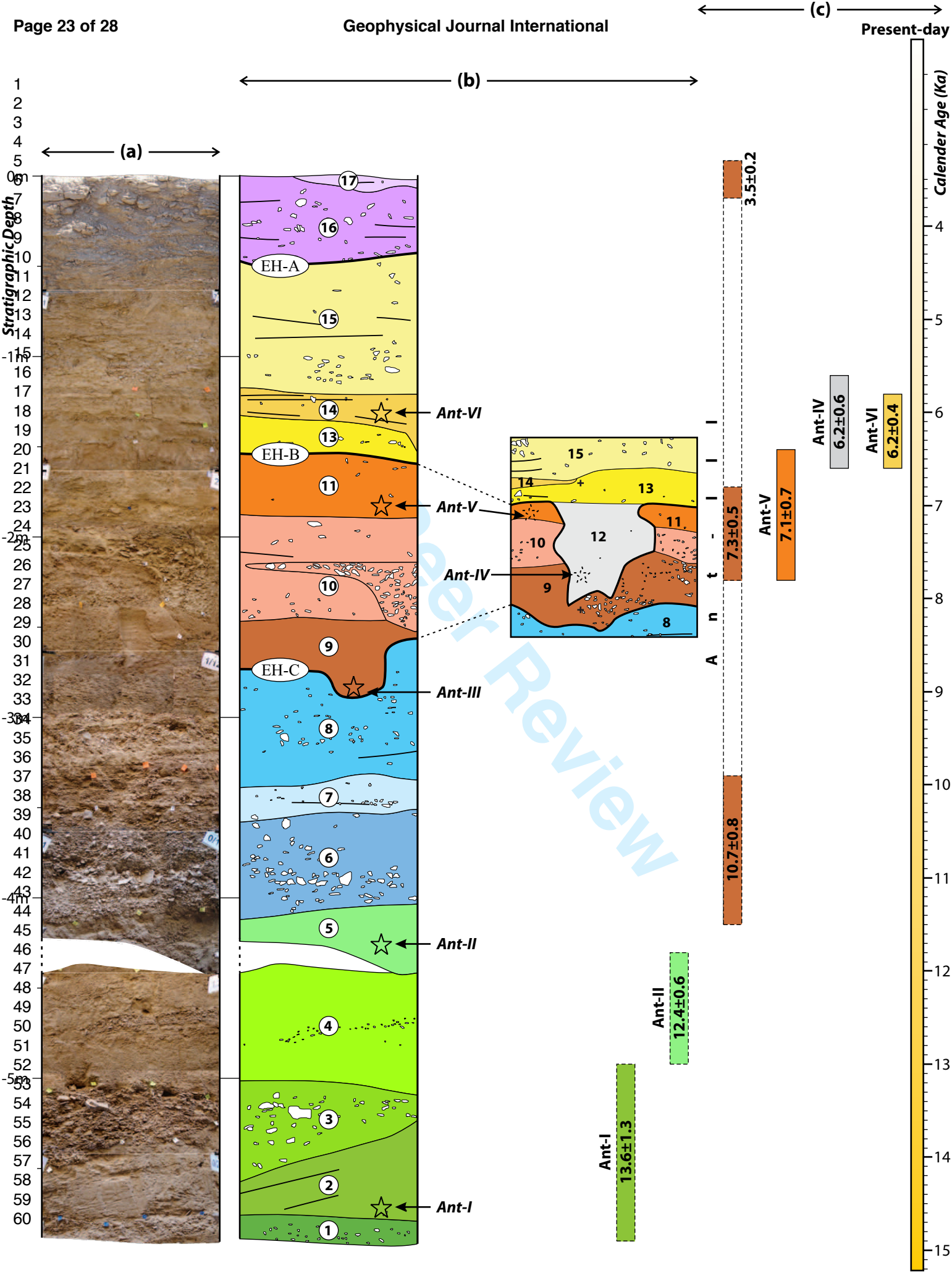
(a)
(b)
(c)
Present-day
Stratigraphic Depth
Calender Age (Ka)
EH-A
EH-B
EH-C
Ant-VI
Ant-V
Ant-IV
Ant-III
Ant-II
Ant-I
Antarctic-I
3.5±0.2
7.3±0.5
10.7±0.8
Ant-V
7.1±0.7
Ant-IV
6.2±0.6
Ant-VI
6.2±0.4
Ant-II
12.4±0.6
Ant-I
13.6±1.3

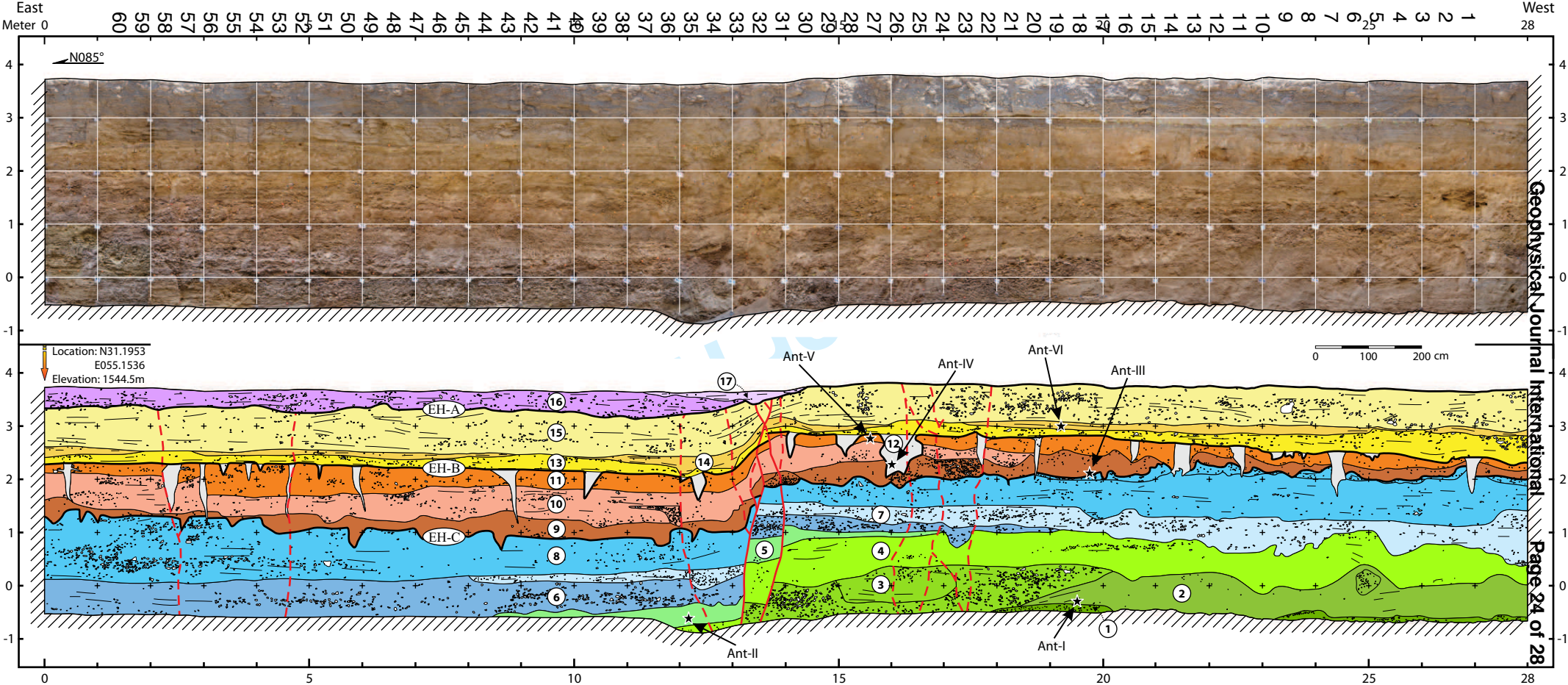
East
Meter 0
West
28
N085°
Location: N31.1953
E055.1536
Elevation: 1544.5m
0 100 200 cm
EH-A
EH-B
EH-C
Ant-V
Ant-IV
Ant-VI
Ant-III
Ant-II
Ant-I
Geophysical Journal International
Page 24 of 28

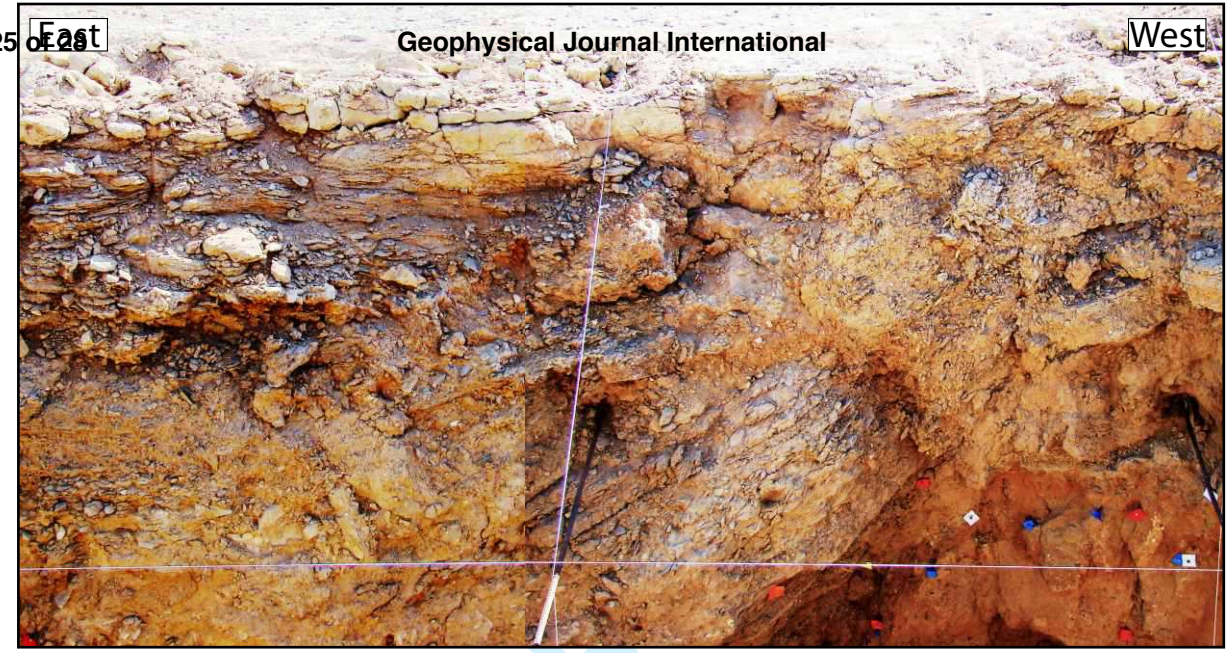
East
West
Meter 12
0
50
100
CENTIMETERS
14

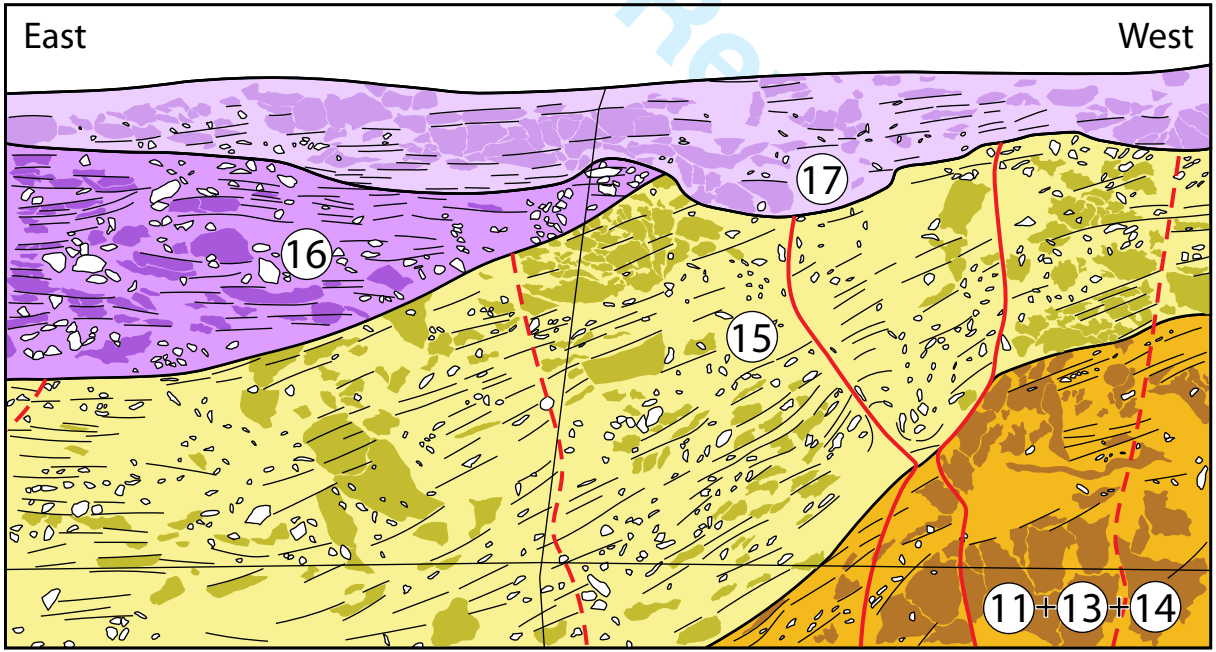
East
West
17
16
15
11+13+14

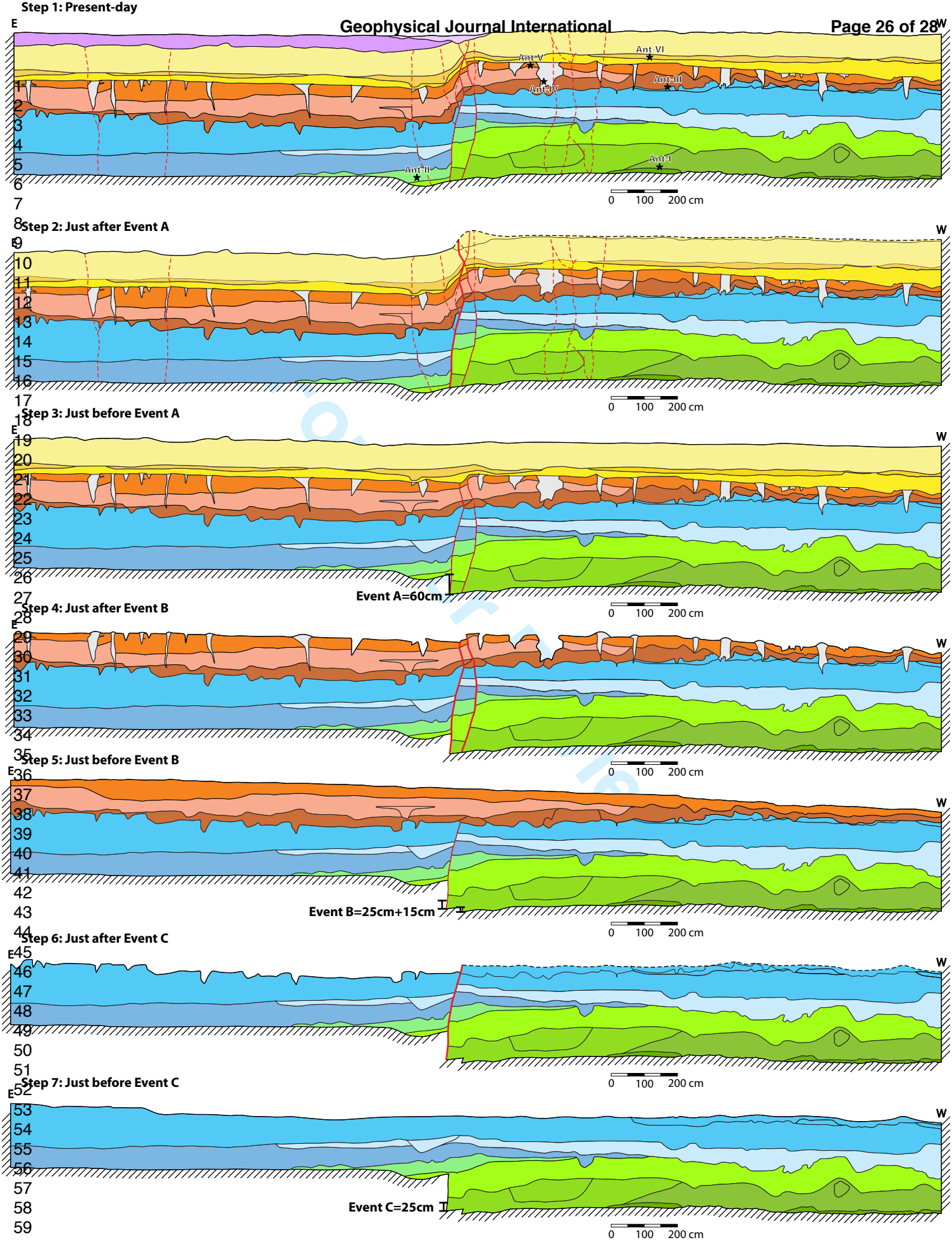
Step 1: Present-day
E
W
Ant-V
Ant-VI
Ant-IV
Ant-III
Ant-II
Ant-I
0 100 200 cm
Step 2: Just after Event A
E
W
0 100 200 cm
Step 3: Just before Event A
E
W
Event A=60cm
0 100 200 cm
Step 4: Just after Event B
E
W
0 100 200 cm
Step 5: Just before Event B
E
W
Event B=25cm+15cm
0 100 200 cm
Step 6: Just after Event C
E
W
0 100 200 cm
Step 7: Just before Event C
E
W
Event C=25cm
0 100 200 cm

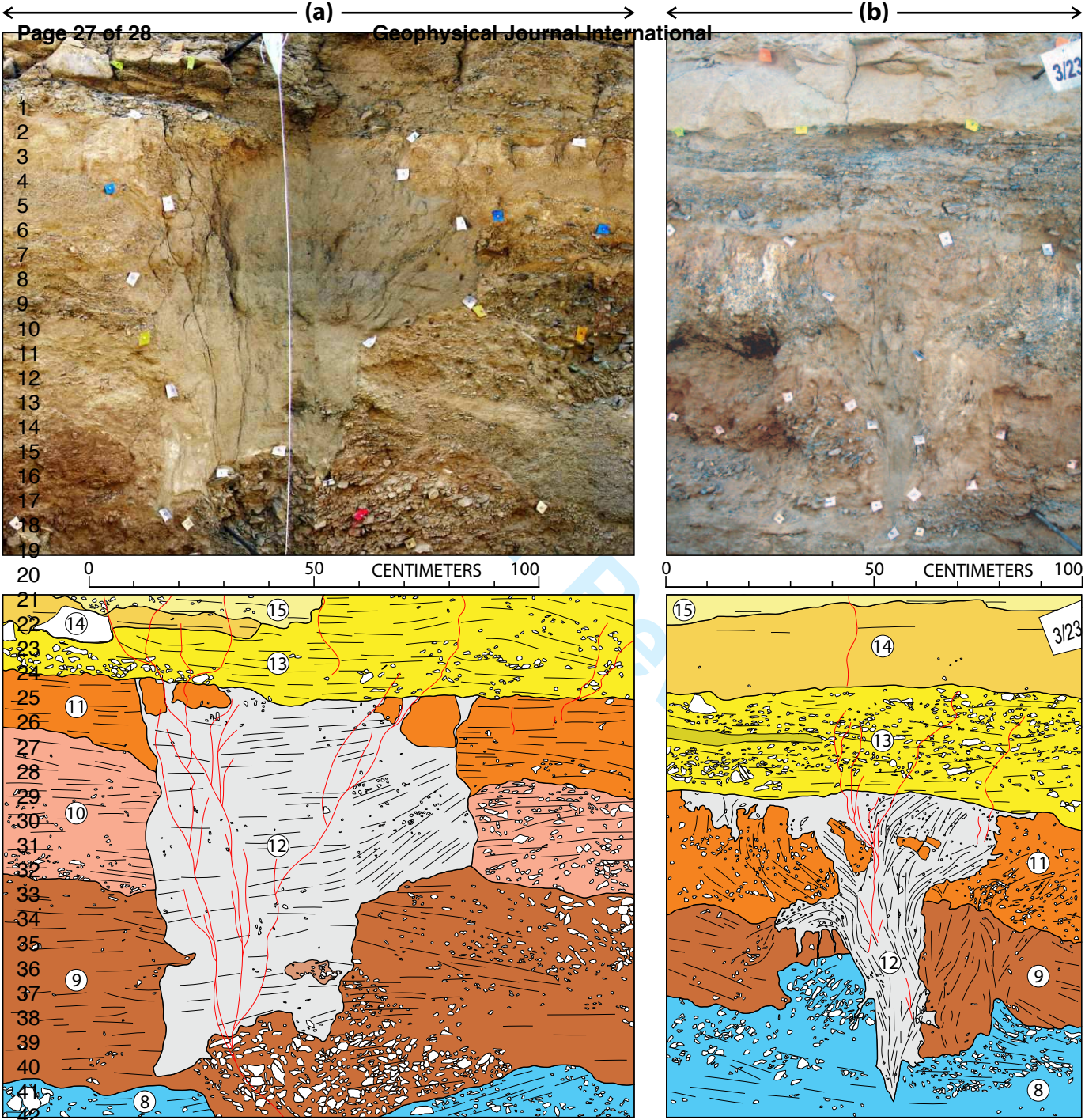
(a)
(b)
CENTIMETERS
0
50
100
3/23
8
9
10
11
12
13
14
15

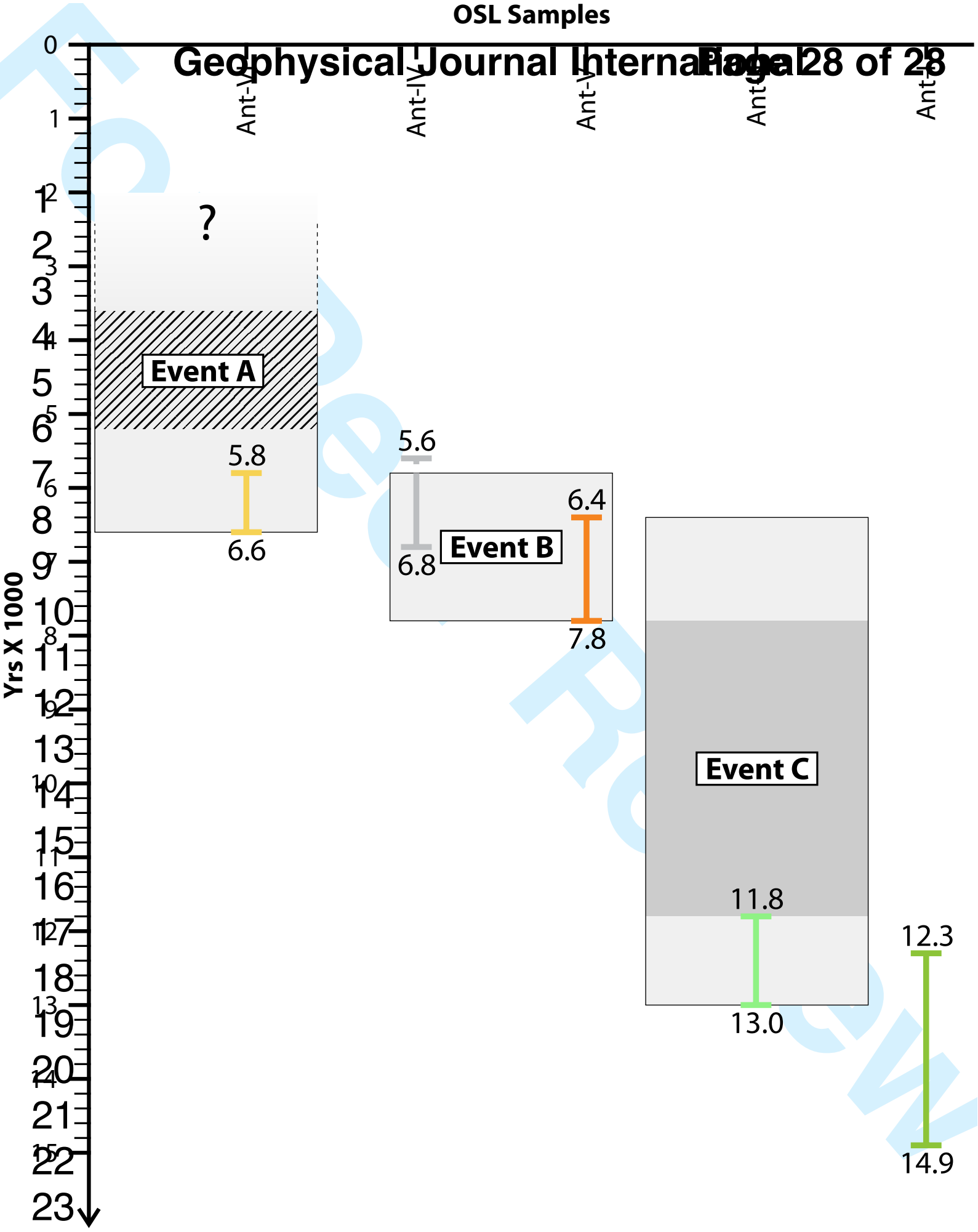
OSL Samples
Ant-V
Ant-IV
Ant-V
Ant-V
Ant-V
Yrs X 1000
0
1
2
3
4
5
6
7
8
9
10
11
12
13
14
15
16
17
18
19
20
21
22
23
?
Event A
5.8
6.6
5.6
6.8
Event B
6.4
7.8
Event C
11.8
13.0
12.3
14.9